nature

https://doi.org/10.1038/s41586-019-1800-4

Supplementary information

Phonon heat transfer across a vacuum through quantum fluctuations

In the format provided by the authors and unedited

King Yan Fong, Hao-Kun Li, Rongkuo Zhao, Sui Yang, Yuan Wang & Xiang Zhang

Supplementary Information for

Phonon heat transfer across a vacuum through quantum fluctuations

King Yan Fong[1]*, Hao-Kun Li[1]*, Rongkuo Zhao[1], Sui Yang[1], Yuan Wang[1], Xiang Zhang[1,2]†

[1]Nanoscale Science and Engineering Center, University of California, Berkeley, CA 94720, USA.

[2]University of Hong Kong, Hong Kong, China

†Correspondence to: xiang@berkeley.edu *These authors contributed equally.

Contents

1. Theoretical analysis of heat transfer induced by the Casimir interaction

Consider two parallel plates separated by a distance d (Fig. S1). Within the region $-L_i/2 < x, y < L_i/2$ (i = 1, 2), the membrane can make vertical displacement $u_i(x, y)$. The two membranes are connected to thermal baths at temperatures T_1 and T_2.

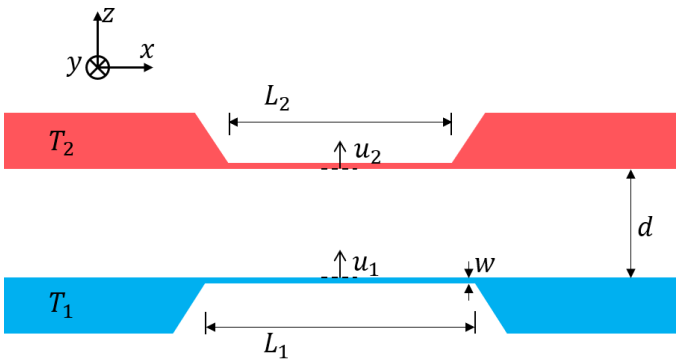

Figure S1 | Schematics of the structure under theoretical consideration.

Because of the quantum fluctuations of the electromagnetic field, there exists Casimir force acting between the two membranes. The dynamic equations for the two membranes with built-in tensile stress are given by

Q1a

$$\sigma_1 \nabla^2 u_1(x,y,t) + F_{Cas}[u_1(x,y,t), u_2(x',y',t)]/w = \rho \frac{\partial^2 u_1(x,y,t)}{\partial t^2} \quad \text{(S1a)}$$

$$\sigma_2 \nabla^2 u_2(x,y,t) + F_{Cas}[u_2(x,y,t), u_1(x',y',t)]/w = \rho \frac{\partial^2 u_2(x,y,t)}{\partial t^2} \quad \text{(S1b)}$$

Assume that the two membranes have the same density ρ and thickness w but different stress σ_1 and σ_2. The stress depends on the bulk temperatures and therefore can be thermally controlled. F_{Cas} represents the Casimir force ***per area***, which is a functional of the displacement profile of both membranes. In the regime where the motions of the membranes are much slower than the

response time of the Casimir interaction, the Casimir force acts instantaneously. Using the Proximity Force Approximation [1] and expanding the force to the first order, we obtain

$$\sigma_1 \nabla^2 u_1(x,y,t) + F'_{Cas}(d)\big(u_1(x,y,t) - u_2(x,y,t)\big)/w = \rho \frac{\partial^2 u_1(x,y,t)}{\partial t^2} \tag{S2a}$$

$$\sigma_2 \nabla^2 u_2(x,y,t) + F'_{Cas}(d)\big(u_2(x,y,t) - u_1(x,y,t)\big)/w = \rho \frac{\partial^2 u_2(x,y,t)}{\partial t^2} \tag{S2b}$$

where the constant force term is neglected. For tensile-stressed membranes, the fundamental eigenmode profile is given by

Q1b

$$u_i(x,y,t) = \begin{cases} u_i(t)\cos\left(\frac{\pi x}{L_i}\right)\cos\left(\frac{\pi y}{L_i}\right), & |x|,|y| < \frac{L_i}{2} \\ 0, & \text{otherwise} \end{cases} \tag{S3}$$

where $i \in \{1,2\}$. When the Casimir force is small compared to the stress force, its existence does not alter the mode profile. Integrating the eigenmode profile on both sides of the equations, we obtain

Q1c

$$-\frac{\pi^2 \sigma_1 u_1}{2} + \frac{F'_{Cas}(d)}{w}\left(\frac{L_1^2 u_1}{4} - \frac{L_1^2 \alpha_1 u_2}{4}\right) = \rho \frac{L_1^2 \ddot{u}_1}{4} \tag{S4a}$$

$$-\frac{\pi^2 \sigma_2 u_2}{2} + \frac{F'_{Cas}(d)}{w}\left(\frac{L_2^2 u_2}{4} - \frac{L_2^2 \alpha_2 u_1}{4}\right) = \rho \frac{L_2^2 \ddot{u}_2}{4} \tag{S4b}$$

where the correction factors α_1, α_2 accounts for the mode profile mismatch, i.e.,

$$\alpha_i = \frac{4}{L_i^2}\left[\int_{-\frac{\min\{L_1,L_2\}}{2}}^{\frac{\min\{L_1,L_2\}}{2}} dx \cos\frac{\pi x}{L_1}\cos\frac{\pi x}{L_2}\right]^2 \tag{S5}$$

The two coupled equations can be rewritten as

Q1d

$$\ddot{u}_1 + \Omega^2 u_1 - 2\Omega g_C(u_1 - \alpha_1 u_2) = 0 \quad \text{(S6a)}$$

$$\ddot{u}_2 + \Omega^2 u_2 - 2\Omega g_C(u_2 - \alpha_2 u_1) = 0 \quad \text{(S6b)}$$

where $\Omega_i = \sqrt{\frac{2\sigma_i}{\rho}}\frac{\pi}{L_i}$ are the resonance frequencies, and frequency matching $\Omega = \Omega_1 = \Omega_2$ through thermal control of the stress is assumed. The coupling rate g_C is given by $g_C = F'_{Cas}(d)/2\Omega\rho w$, or

$$g_C = \frac{F'_{Cas}(d)}{2\Omega\rho_A} \quad \text{(S7)}$$

where $\rho_A = \rho w$ is the area density (mass per area). A remark here is that when only one membrane is allowed to move, presence of Casimir force causes the membrane resonance frequency to shift by g_C (taking $u_2 = 0$ in Eq. (S6a)). This frequency shift is used as a correction to obtain the pure thermal radiation effect in Extended Data Fig. 7.

Q1e

We use the Langevin equation to describe thermal fluctuation and dissipation

Q2a

$$\ddot{u}_1 + 2\gamma_1\dot{u}_1 + \Omega^2 u_1 - 2\Omega g_C(u_1 - \alpha_1 u_2) = \frac{\delta F_1}{m_1} \quad \text{(S8a)}$$

$$\ddot{u}_2 + 2\gamma_2\dot{u}_2 + \Omega^2 u_2 - 2\Omega g_C(u_2 - \alpha_2 u_1) = \frac{\delta F_2}{m_2} \quad \text{(S8b)}$$

where the fluctuating forces are related to the bath temperatures T_i and mechanical dampings γ_i by $\langle \delta F_i(t)\delta F_j(t')\rangle = \delta_{ij}\delta(t-t')8k_B T_i\gamma_i m_i$. The effective mass m_i is given by one quarter of the total mass of the resonator, i.e., $m_i = L_i^2\rho_A/4$. Using the quadrature notations in the rotating frame defined as $q(t) = \left[\tilde{q}(t)e^{-i\Omega t} + \tilde{q}^*(t)e^{i\Omega t}\right]/2$ for $q \in \{u_1, u_2, \delta F_1, \delta F_2\}$ and assuming $\gamma_i \ll \Omega$, we obtain

$$\dot{\tilde{u}}_1 + \gamma_1 \tilde{u}_1 - i g_C(\tilde{u}_1 - \alpha_1 \tilde{u}_2) = \frac{i\delta \tilde{F}_1}{2\Omega m_1} \tag{S9a}$$

$$\dot{\tilde{u}}_2 + \gamma_2 \tilde{u}_2 - i g_C(\tilde{u}_2 - \alpha_2 \tilde{u}_1) = \frac{i\delta \tilde{F}_2}{2\Omega m_2} \tag{S9b}$$

In the frequency domain, they become

$$\begin{pmatrix} \omega + g_C + i\gamma_1 & -g_C\alpha_1 \\ -g_C\alpha_2 & \omega + g_C + i\gamma_2 \end{pmatrix} \begin{pmatrix} \tilde{u}_1[\omega] \\ \tilde{u}_2[\omega] \end{pmatrix} = -\frac{1}{2\Omega} \begin{pmatrix} \delta \tilde{F}_1[\omega]/m_1 \\ \delta \tilde{F}_2[\omega]/m_2 \end{pmatrix} \tag{S10}$$

Eigen-frequencies of the coupled modes can be solved by taking determinant of the matrix on the left-hand-side to be zero. The eigen-frequencies are given by

$$\omega_{\pm} = -g_C \left[1 \pm \sqrt{\alpha_1\alpha_2 - (\gamma_1 - \gamma_2)^2/g_C^2} \right] - i\frac{\gamma_1 + \gamma_2}{2} \tag{S11}$$

As the two membranes are close to size-matched, $\alpha_1\alpha_2$ approaches 1. In our experiment, $L_1 = 330$ μm and $L_2 = 280$ μm leads to $\alpha_1\alpha_2 = 0.95$. When the two oscillators are strongly coupled, i.e., $g_C \gg \gamma_1, \gamma_2$, the eigen-frequencies in the non-rotating frame become

$$\Omega_{even} \approx \Omega - g_C\left(1 - \sqrt{\alpha_1\alpha_2}\right) - i(\gamma_1 + \gamma_2)/2 \tag{S12a}$$

$$\Omega_{odd} \approx \Omega - g_C\left(1 + \sqrt{\alpha_1\alpha_2}\right) - i(\gamma_1 + \gamma_2)/2 \tag{S12b}$$

The even (odd) mode corresponds to the coupled mode where the two resonators move in same (opposite) direction (see Fig. 4a inset for illustration). The frequency splitting is given by

$$\Delta\Omega = 2g_C' \quad \text{or} \quad \Delta f = g_C'/\pi \tag{S13}$$

where $g_C' = g_C\sqrt{\alpha_1\alpha_2}$ is the effective coupling rate that includes the mode-matching correction. In our experiment, $\sqrt{\alpha_1\alpha_2} = 0.97$ and therefore $g_C' \approx g_C$. Strength of the coupling is determined by the ratio $g_C'^2/\gamma_1\gamma_2$. Note that Δf is a direct measure of the Casimir force gradient.

To derive temperature of the phonon mode, we obtain the power spectral densities from Eq. (S10) as

$$S_{\tilde{u}_1^*\tilde{u}_1}[\omega] = \frac{[(\omega+g_C)^2+\gamma_2^2]2k_BT_1\gamma_1/m_1 + g_C^2\alpha_1^2 2k_BT_2\gamma_2/m_2}{\Omega^2[[(\omega+g_C)^2-\gamma_1\gamma_2-g_C'^2\,]^2+(\gamma_1+\gamma_2)^2(\omega+g_C)^2]} \tag{S14a}$$

$$S_{\tilde{u}_2^*\tilde{u}_2}[\omega] = \frac{[(\omega+g_C)^2+\gamma_1^2]2k_BT_2\gamma_2/m_2 + g_C^2\alpha_2^2 2k_BT_1\gamma_1/m_1}{\Omega^2[[(\omega+g_C)^2-\gamma_1\gamma_2-g_C'^2\,]^2+(\gamma_1+\gamma_2)^2(\omega+g_C)^2]} \tag{S14b}$$

The mean square fluctuation of the displacement is related to the spectral densities by $\langle|\tilde{u}_i|^2\rangle = \int_{-\infty}^{\infty} d\omega\, S_{\tilde{u}_i^*\tilde{u}_i}[\omega]/2\pi$. Using $k_BT_i' = m_i\Omega^2\langle u_i^2\rangle$, the mode temperatures can be expressed as

$$T_1' = \int_{-\infty}^{\infty}\frac{d\omega}{\pi}\frac{[(\omega+g_C)^2+\gamma_2^2]T_1\gamma_1 + g_C'^2T_2\gamma_2}{[(\omega+g_C)^2-\gamma_1\gamma_2-g_C'^2\,]^2+(\gamma_1+\gamma_2)^2(\omega+g_C)^2} \tag{S15a}$$

$$T_2' = \int_{-\infty}^{\infty}\frac{d\omega}{\pi}\frac{[(\omega+g_C)^2+\gamma_1^2]T_2\gamma_2 + g_C'^2T_1\gamma_1}{[(\omega+g_C)^2-\gamma_1\gamma_2-g_C'^2\,]^2+(\gamma_1+\gamma_2)^2(\omega+g_C)^2} \tag{S15b}$$

The above integrals can be carried out analytically and simplified as

$$T_1' = T_1 + \frac{\gamma_2(T_2-T_1)}{(\gamma_1+\gamma_2)\left(1+\frac{\gamma_1\gamma_2}{g_C'^2}\right)} \tag{S16a}$$

$$T_2' = T_2 + \frac{\gamma_1(T_1-T_2)}{(\gamma_1+\gamma_2)\left(1+\frac{\gamma_1\gamma_2}{g_C'^2}\right)} \tag{S16b}$$

In the weak and strong coupling regimes, we have

Q2b

Case 1: $g_C \ll \gamma_1, \gamma_2$ (weak coupling)

$$T_1' = T_1 \quad \text{and} \quad T_2' = T_2 \tag{S17}$$

Case 2: $g_C \gg \gamma_1, \gamma_2$ (strong coupling)

$$T_1' = T_2' = T_{th}' = \frac{T_1\gamma_1 + T_2\gamma_2}{\gamma_1 + \gamma_2} \tag{S18}$$

Note that $g_C \propto F_{Cas}'(d) \propto d^{-5}$, therefore, the Casimir heat transfer effect rises sharply at short distance.

Net energy flow rate from the thermal bath to the mode can be calculated from

$$P_i = \langle(\delta F_i - 2\gamma_i m_i \dot{u}_i) \cdot \dot{u}_i\rangle = 2\gamma_i k_B (T_i - T_i') \tag{S19a}$$

which leads to

$$P_2 = -P_1 = \frac{2\gamma_1\gamma_2 k_B (T_2 - T_1)}{(\gamma_1 + \gamma_2)\left(1 + \frac{\gamma_1\gamma_2}{g_C'^2}\right)} \tag{S19b}$$

The expression is consistent with the results of Ref. 2 (See Eq. (43) of Ref. 2). In the limit of strong coupling ($g_C \gg \gamma_1, \gamma_2$), we obtain

$$P_2 = -P_1 = \frac{2\gamma_1\gamma_2}{\gamma_1 + \gamma_2} k_B (T_2 - T_1) = \frac{\Omega}{Q_1 + Q_2} k_B (T_2 - T_1) \tag{S20}$$

In the above analysis, proximity force approximation was used which treats the membrane surfaces as parallel planes locally. Such an approximation is valid when the wavelength of the phonon mode is much larger than the gap, i.e., $d/\lambda \ll 1$. In our experiment, $\lambda = 2L \approx 600$ μm and $d/\lambda \approx 10^{-3}$, and thus the condition is satisfied. When the condition is no longer valid,

correction of the Casimir interaction will be necessary as discussed in Refs. [3,4]. In the following we estimate such a correction in our experiment.

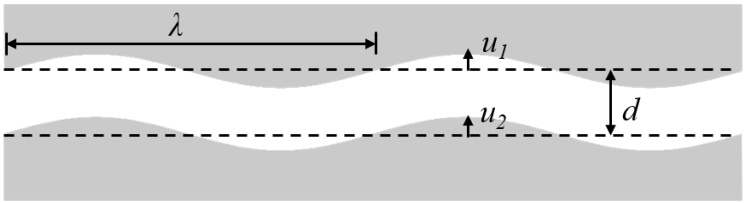

Figure S2 | Surface modulation in presence of phonon.

Consider phonon modes with amplitudes u_1 and u_2 and wavelength λ excited on two parallel surfaces separated by a short distance d, as illustrated in Fig. S2. Compared to the perfectly planar configuration, the surface modulation due to phonons modifies the vacuum energy. Ref. 3 derives the modification of the van der Waal's energy per area as (see Eqs. (16) & (23) of Ref. 3)

$$\Delta E_{vdW} = -\frac{C\pi}{8d^4}\left[(u_1 - u_2)^2 + 2\pi^2\left(\frac{d}{\lambda}\right)^2 u_1 u_2\right] \qquad (S22)$$

where $d/\lambda \ll 1$ is assumed to expand the expression to the lowest order of d/λ. The first term is the spring term that expresses the coupling between the two phonon modes. The second term is the cross term which has a coefficient on the order of 10^{-5} under our experimental condition.

A similar expression for Casimir energy that takes into account the retardation effect can be obtained from Ref. 4. By combining and expanding Eqs. (44), (32), (37), (38), (46), (50a), and (50b) of Ref. 4 to the lowest order of d/λ and noticing that $\mathcal{E}_{cc}(b = 0) \propto u_1 u_2$ for situation $u_1 \neq u_2$, the modification of the Casimir energy per area can be expressed as

$$\Delta E_{Cas} = -\frac{\hbar c\pi^2}{240d^5}\left\{(u_1-u_2)^2\left[1-\frac{60-4\pi^2}{9}\left(\frac{d}{\lambda}\right)^2\right]+\frac{4\pi^2}{3}\left(\frac{d}{\lambda}\right)^2 u_1u_2\right\} \quad (S23)$$

In this case, both the spring term ($\propto (u_1-u_2)^2$) and the cross term ($\propto u_1u_2$) contain correction terms that are of the second-order of d/λ. Those terms are on the order of 10^{-5} under our experimental condition.

2. Thermal time constants of the bulk and single-mode heat transfer

Here we analyze the thermal time constants of both the bulk and single-mode heat transfer processes in our system. For bulk processes (Fig. S3a), thermal time constants for radiation heat transfer (τ_{rad}) and heat dissipation to substrate (τ_{dis}) are estimated by $\tau_{rad} = (h_{Au}C_{Au} + h_{SiN}C_{SiN})/\kappa_{rad}(d)$ and $\tau_{dis} = L^2(h_{Au}C_{Au} + h_{SiN}C_{SiN})/4(h_{Au}\kappa_{Au} + h_{SiN}\kappa_{SiN})$, where h_{Au} (h_{SiN}), C_{Au} (C_{SiN}), and κ_{Au} (κ_{SiN}) represent the thickness, heat capacitance (per volume) and thermal conductivity of the gold (silicon nitride) thin film. $\kappa_{rad}(d) = 1.4$ (300 nm/d)$^{2.46}$ Wm^2/K is the thermal radiation conductance between gold surfaces determined experimentally in Ref. 5. For single-mode processes (Fig. S3b), thermal time constants for the resonant Casimir heat transfer (τ_C) and heat dissipation to thermal bath (τ_i) are given by $\tau_C = 1/g_C(d)$ and $\tau_i = 1/\gamma_i$ ($i = 1,2$). Values of the parameters used in calculation are $\{C_{Au}, C_{SiN}\} = \{2.5, 1.6\}\times 10^6$ J/m^{3}K, $\{\kappa_{Au}, \kappa_{SiN}\} = \{150, 10\}$ W/mK, $\{h_{Au}, h_{SiN}\} = \{150, 100\}$ nm, and $L = 300$ μm.

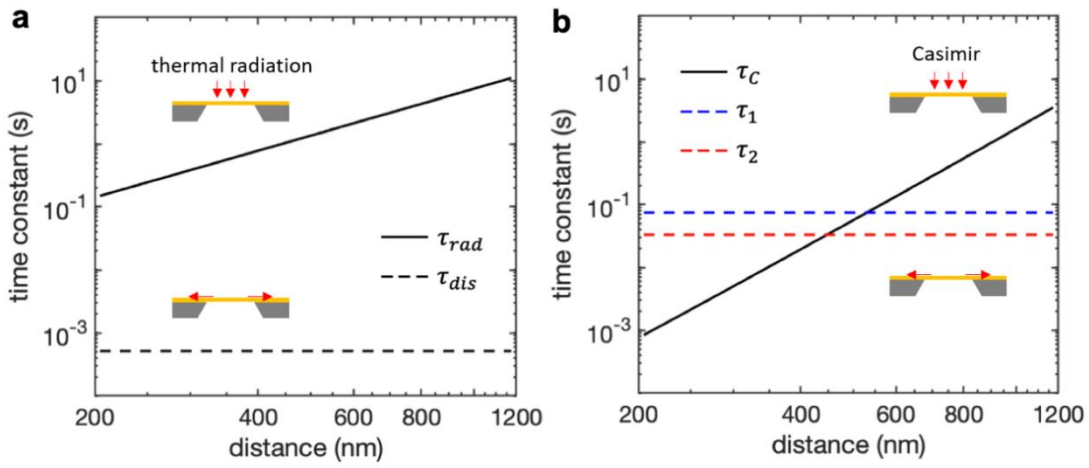

Figure S3 | Thermal time constants for bulk (**a**) and single-mode (**b**) heat transfer processes.

We can see that $\tau_{rad} \gg \tau_{dis}$ in all distances. It means that thermal radiation is not effective in influencing the membrane temperature since heat dissipates to substrate faster. On the other hand, $\tau_C \ll \tau_1, \tau_2$ at short distance meaning that Casimir effect is efficient in transferring heat. This is the main reason why the Casimir effect can significantly change the mode temperature and lead to thermalization at short distance. Also, we can see that $\tau_C < \tau_{rad}$ for the whole distance range and therefore the Casimir heat transfer effect occurs faster than thermal radiation. Another remark is that both τ_{rad} and τ_{dis} are much larger than the membrane oscillation period $1/\Omega \sim 1$ μs, therefore, the membrane bulk temperature could not fluctuate fast enough to excite the membrane resonance.

3. Stabilities of the bias voltage and mechanical damping

Throughout the heat transfer measurement, the bias voltage V_b is applied to compensate for the surface potential V_0 at each separation. We apply the bias voltage by connecting a low-noise

source meter (Keithley 2400) to the sample through an RC circuit shown in Fig. S4a. The circuit serves as a potential divider and low-pass filter. It provides a dividing ratio of 45 dB at DC and 62 dB at 200 kHz. To estimate the fluctuation in V_b, we measure the noise spectral density of the source meter ($\overline{v_s^2}/\Delta f$). The results are shown below in Figs. S4b & S4c. We estimate that ($\overline{v_b^2}/\Delta f$) reaches the thermal Johnson noise $S_v(\omega) = \frac{4k_BT(R_1\|R_2)}{1+\omega^2(R_1\|R_2)^2C^2}$ at low frequency above 30 Hz with $S_v \approx 1 \times 10^{-18}$ V^2/Hz (except at the harmonics of AC power line frequency 60 Hz) and at frequency near the membrane resonance with $S_v \approx 2 \times 10^{-20}$ V^2/Hz.

The voltage difference between the two membranes is given by $[(\overline{V_b} - V_0) + v_b(t)]$. The residual voltage $(\overline{V_b} - V_0)$ is estimated to be <5 mV based on the measurement precision in determining V_0 (see Extended Data Fig. 5b). The fluctuation voltage is much smaller than the residual voltage, namely $v_b(t) \ll (\overline{V_b} - V_0)$, and thus the electrostatic force per area can be written as $F_E(t) = -\varepsilon_0(\overline{V_b} - V_0)[(\overline{V_b} - V_0) + 2v_b(t)]/2d^2$.

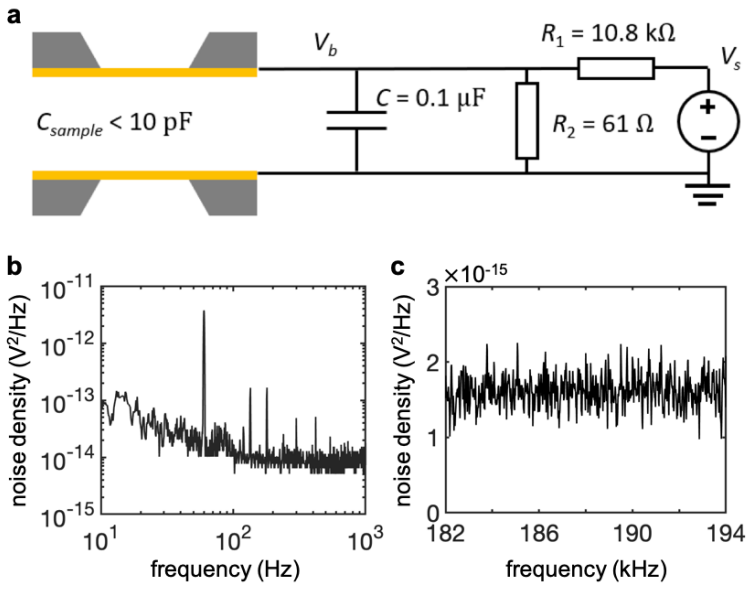

Figure S4 | a, Electrical circuit for applying the bias voltage. **b**, **c**, Noise power density of the source meter at low frequency (**b**) and at frequency near the membrane resonance (**c**), respectively.

In the low frequency range, the fluctuation of the electrostatic force would cause drift of the electrostatic coupling between the membranes. In Fig. S5a, we compare the Casimir coupling rate g_C (induced by the Casimir force), residue electrostatic coupling rate g_E (caused by $\bar{V}_b - V_0$), and the electrostatic coupling fluctuation Δg_E (using $\sqrt{\langle v_b^2 \rangle} = \sqrt{k_B T/C}$). It is shown that both g_E and Δg_E are several orders of magnitude smaller than g_C, and thus are negligible.

In the high frequency range near the mechanical resonance, the fluctuation of the electrostatic force would resonantly drive and thus heat up the mechanical modes. In Fig. S5b, we present the calculated temperature rise of the two mechanical modes $\Delta T_1'$ and $\Delta T_2'$ using the estimated noise density near the mechanical resonance frequency. Above 300 nm, the mode temperature rise is less than 0.001 K, which is negligible.

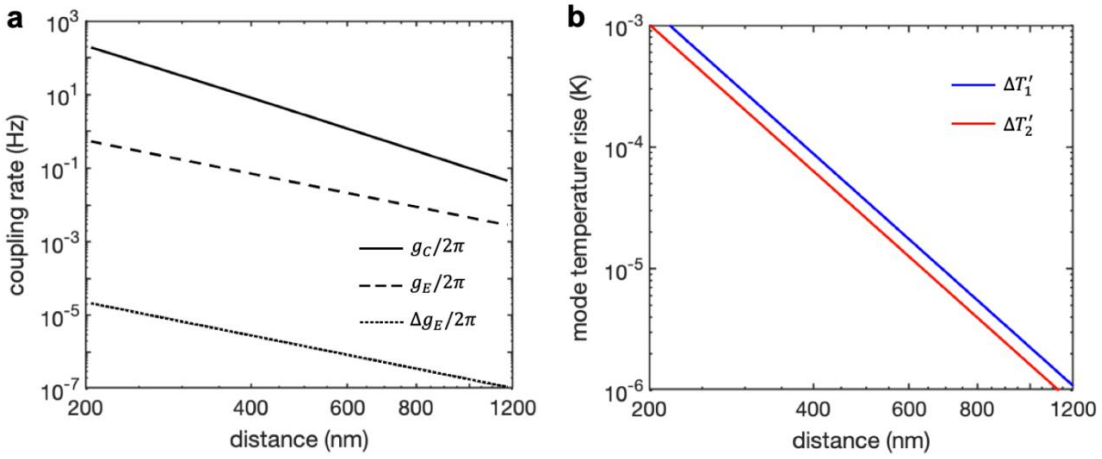

Figure S5 | a, Comparison of the Casimir coupling rate g_C, the residue electrostatic coupling rate g_E, and the electrostatic coupling fluctuation Δg_E. **b**, Estimated mode temperature rise induced by bias voltage fluctuations.

References

1. Błocki, J., Randrup, J., Świątecki, W. J., & Tsang, C. F. Proximity forces. Annals of Physics 105, 427 (1977).

2. Biehs, S.-A. and Agarwal, G. S. Dynamical quantum theory of heat transfer between plasmonic nanosystems. J. Opt. Soc. Am. B 30, 700-707 (2013).

3. Pendry, J. B., Sasihithlu, K., & Craster, R. V. Phonon-assisted heat transfer between vacuum-separated surfaces. Phys. Rev. B 94, 075414 (2016).

4. Emig, T., Hanke, A., Golestanian, R., & Kardar, M. Normal and lateral Casimir forces between deformed plates. Phys. Rev. A 67, 022114 (2003).

5. Shen, S., Mavrokefalos, A., Sambegoro, P., & Chen, G. Nanoscale thermal radiation between two gold surfaces. App. Phys. Lett. 100, 233114 (2012).